Urban fraction influence on local nocturnal cooling rates from low-cost sensors in Dallas-Fort Worth

Braedyn D. McBroom, David A. Rahn [*], Nathaniel A. Brunsell

Department of Geography and Atmospheric Science, University of Kansas, 1475 Jayhawk Blvd, Lawrence 66045, KS, USA

ARTICLE INFO

ABSTRACT

Increased health risks and economic vulnerability are associated with higher nighttime temperatures in urban areas. Urbanization slows cooling overnight, and the heterogeneous built environment leads to inequitable distributions of health risks and cooling costs. Quantifying the relationship between the local built environment and cooling rates of air temperature is typically inhibited by a lack of in situ measurements. There are many new low-cost sensors that primarily measure urban air pollution that also measure air temperature, which permits a more comprehensive examination of the local urban heat island. The Dallas-Fort Worth region is an ideal location and cooling rates of 116 sensors from 2020 to 2022 are linked to the local urban fraction to quantify the impact of the built environment on local air temperature. Days that are not clear and calm are removed to isolate the local forcing from the synoptic forcing. Cooling rates significantly and linearly slow as the urban fraction increases during all months at a rate of 0.5–0.7 $^{\circ}$C hr^{-1} urbfrac^{-1} with the greatest impact occurring in spring and fall. These results provide highly localized relationships that work towards a better understanding of the heterogeneous and inequitable nature of cities that will only improve as the data set grows.

1. Introduction

Urbanization replaces natural land cover with low-albedo impervious surfaces, drastically altering the local radiative balance and energy exchange by reducing evapotranspiration, increasing sensible heat flux, and modifying heat storage (Oke, 1988; Arnfield, 2003). The result is a positive land surface temperature (Tran et al., 2006; Imhoff et al., 2010; Peng et al., 2011) and air temperature anomalies (Oke, 1995; Azevedo et al., 2016) when compared to the rural surroundings known as the urban heat island (UHI, Oke, 1982). The general UHI can be classified and measured at the surface or using the air temperature. The surface UHI can be inferred from remote sensing, the air temperature near the surface represents the canopy layer UHI that is commonly studied and observed through surface station measurements, and the urban boundary layer also contains a UHI signal that can be obtained through remote sensing or in situ with radiosonde and aircraft observations.

The maximum intensity of the UHI typically occurs at night, and during the day urban areas can be slightly cooler than the rural surroundings (Hafner and Kidder, 1999; Morris and Simmonds, 2000; Unwin, 1980; Myrup et al., 1993; Basara et al., 2008). UHIs are amplified by anthropogenic processes, most notably from air conditioning systems, vehicle emissions, and industrial activity (Shahmohamadi et al., 2011; Salamanca et al., 2014). The UHI is related to health risks including heat stress and respiratory illness through its connection to the mixed-layer depth and air pollution. In fact, the UHI accounted for around 50% of the total heat-related mortality

---

* Corresponding author.
E-mail address: darahn@ku.edu (D.A. Rahn).

during the 2003 heatwave in the West Midlands (Heaviside et al., 2016). This implies that continued urbanization and anthropogenic global warming over the next several decades will threaten public health, so it is crucial to understand the characteristics and behavior of the atmosphere over the urban environment.

It is particularly concerning that there is a steady increase of nighttime air temperature across the United States (Zhang et al., 2014). If the minimum morning temperature remains high during the summer months, people are not able to recover, and morbidity and mortality rates increase (e.g., Laaidi et al., 2012). This background warming is amplified at the city scale by the UHI effect. Even between neighborhoods within the same city, the magnitude of the UHI effect can vary greatly in magnitude depending on the local built environment and the amount of green space. Many factors including building configuration (Monaghan et al., 2014), impervious surface area (Imhoff et al., 2010), and vegetation indices (Weng et al., 2011) contribute to the local impacts. Although urban fraction is a simplification of many processes that impact the UHI, it is a useful metric that can be used to account for the impact of the built environment on the structure and magnitude of the UHI (Hu and Brunsell, 2015).

Development within cities is driven by many factors, and this leads to a distribution of heat risk within a city that is inequitable and often places extra burdens on the most vulnerable and already overburdened communities (Chakraborty et al., 2019). The spatial variation of heat risk can be sharp and change drastically from neighborhood to neighborhood, and without a fairly dense network of observations, these sharp contrasts are not able to be measured. This has important consequences since a neighborhood with temperatures much greater than other locations within the city may not be identified or adequately represented, leading to no action being taken by government agencies or community members. For many environmental justice groups, data collection is not optional, and it is necessary to successfully advocate for change (Boston et al., 2023). These same hot spots are also prone to increased economic burdens in the form of higher energy costs due to air conditioning (Akbari et al., 2001).

Satellite observations provide high spatial resolution of surface temperature, which can only be indirectly related to the air temperature that people experience, and can contain sampling biases (e.g., Hu and Brunsell, 2013; Stewart et al., 2021). Standard observations of air temperature, such as the automatic surface observing systems (ASOS) operated by the National Weather Service, are expensive and do not provide dense spatial coverage in urban areas. However, in recent years, the number of low-cost sensors that monitor atmospheric conditions is rapidly increasing. The typical motivation for purchasing and installing these low-cost monitors is to measure air pollution, which are often located in urban areas where communities are concerned with air pollution (Proma et al., 2021).

PurpleAir, Inc. is one company that sells low-cost sensors that measure particulate matter with a pair of optical particle counters, but these sensors also measure temperature, relative humidity, and barometric pressure. While low-cost is a relative term, these sensors are often referred to as low-cost in the literature (e.g., Malings et al., 2020; Stavroulas et al., 2020; Barkjohn et al., 2021). With an onboard Wi-Fi connection, observations are continuously uploaded to a cloud-based platform where both real-time and also archived data are publicly accessible. Given the importance of air pollution, many studies focus on the measurements of particulate matter from this network, but few have leveraged this particular expanding data set for studies related to the UHI.

This work is motivated by the growing number of underutilized, publicly-available, in situ air temperature data within cities that can be used to investigate impacts on local air temperature. Specifically, our objectives are to (1) construct a quality-controlled database of air temperatures to demonstrate its viability in UHI studies, (2) determine local cooling rates relative to sunset to quantify the impact of local urban fraction, (3) demonstrate seasonal shifts in this relationship, and (4) offer ways forward to further exploit this growing set of measurements. This is one of the first studies to examine nocturnal UHI impacts using a dataset that was developed to address environmental issues (air pollution) in traditionally marginalized areas.

2. Data

2.1. PurpleAir

PurpleAir sensors use a pressure–temperature–humidity sensor (Bosch BME280), which is highly reliable, and spurious measurements are rare, on the order of 1 in 10^6 (Barkjohn et al., 2021). Outliers more than three standard deviations were flagged for visual inspection, resulting in the removal of 23 abnormally high observations. Indoor monitors were also easily identified and removed. Given that the primary reason for installing these sensors is to monitor air pollution, many studies concentrate on the quality of the particulate matter measurements. However, some studies also include supplementary information on the quality of temperature measurements, which show robust and highly correlated temperature data (Stavroulas et al., 2020). In fact, the temperature data is often used as a correction factor for the particulate matter measurements (Barkjohn et al., 2021). One of the advantages of PurpleAir sensors is that they are ventilated and have two active fans that draw air in for the laser particle counters. This is in contrast to other low-cost sensors that are sealed and unventilated, which can be an issue for temperature measurements (Chapman et al., 2017). Given each measuring system will have its own strengths and limitations, it would be worthwhile to integrate multiple systems together to assess their performance and create a multi-system network. This work focuses on just one, PurpleAir, which has temperature measurements that have been underutilized. However, future studies would benefit from such a cross-system analysis.

Given that the founding principles for PurpleAir are 'openness, sharing, and community', the data from each station is uploaded in real-time to the cloud and all of the data is publicly available through their API.[1] Environmental justice groups often use PurpleAir to monitor air pollution in overburdened communities. Cumulative impacts of environmental stressors are a great concern to people

---

living in underserved locations where there is both elevated air pollution and an enhanced UHI. Therefore, PurpleAir sensors have the advantage of also being placed in some of the most vulnerable areas.

The Dallas-Fort Worth region is an ideal location for this analysis since it is a large urban area and the weather is not confounded by any major topographic or coastal influences that could overshadow local forcing. Given the continued urbanization of the two cities, the impact of the growing built environment will only intensify in the future. The area is also prone to droughts and heat waves that are associated with significant health and economic impacts.

All available hourly station data from PurpleAir's API during 2020–2022 were obtained in the Dallas-Fort Worth region (97.6–96.6ºW; 32.2–33.6ºN), which included 227 unique sensors. Indoor sensors and sensors that had less than four months of data were excluded, many of those were just installed at the end of the period, leaving 116 sensors. Over time, sensors have to be reset, lose connection, or simply fail, so at any given time, there are fewer concurrently active sensors. The number of observations grew to around 80 concurrently active stations in 2022, which are located in a range of urban fractions (Fig. 1). The period that is used for this study begins in 2020 since the most rapid increase in the number of sensors occurs during 2020. Prior to this time, there were about ten or fewer concurrently operating stations.

2.2. Ancillary

To supplement the low-cost temperature sensors, we use the ASOS stations at the Dallas–Fort Worth International Airport (DFW) and Dallas Love Field Airport (DAL) that provide additional observations of wind and cloud cover. All measurements at these two ASOS stations are generally highly correlated since they are only located 18 km apart (Nielsen and Rahn, 2022). To provide a single regional estimate of wind and cloud cover, observations from these two stations are averaged to create a single hourly time series, which also allows filling of the occasionally missing observation from one airport.

Urban fraction is obtained from the 30-m National Land Cover Database (Dewitz, 2021) and is defined by the percentage of urban impervious surface, which is commonly done (e.g., Wong et al., 2019; He et al., 2023). The urban fraction associated with each station is taken from the nearest neighbor value. The distribution of urban fraction of Dallas-Forth Worth is typical of many major cities in the United States with higher fractions found near the core of the two cities and diminishing outwards (Fig. 2). Even though the stations are not evenly distributed throughout the city, there is broad coverage across many neighborhoods and in rural areas outside of the city that provides ample samples of different urban fractions (Fig. 1b).

3. Methods

Nocturnal cooling rates are obtained from the hourly observations using a span of five hours with the beginning of the nocturnal period defined as the first hourly report after sunset. For each station on each night, a robust linear regression was fit to this five-hour time series of temperature (HuberRegressor, Huber and Ronchetti, 2011). A robust linear regression is chosen since it is less sensitive to outliers than standard least squares linear regression. The cooling rate for the night is the slope of this robust linear regression fit. The daily data are aggregated at time scales of a month and also seasonally as December–February (DJF), March–May (MAM), June–August (JJA), and September–November (SON). Given that the results naturally clustered seasonally and for the sake of brevity, most of the results are presented here as seasonal.

To isolate the impact of local forcing from transient weather events on the nocturnal cooling rates, the wind speed and cloud cover from the ASOS stations are also obtained during the nocturnal period and are averaged over the 5-h time period. The distributions of the average wind speed and cloud cover for all nights from 2020 to 2022 are shown in Fig. 3. Calm and clear nights are defined as an average wind speed less than or equal to 3 m s⁻¹ and an average cloud cover that is less than or equal to 2 oktas. These thresholds strike a balance between retaining a large sample size and effectively removing transient weather events. Using different combinations of reasonable thresholds did not significantly impact the results.

To illustrate the impact of urban fraction on the local cooling rate, monitor 12,969 with an urban fraction of 0.6 and monitor 87,485 with an urban fraction of 0.0 are used to represent sensors located in locations with high and low urban fractions. Temperatures during the nocturnal window are obtained for spring (MAM) when it is clear and calm, and then the temperatures are normalized by removing the mean temperature over the nocturnal period (Fig. 4). Box plots represent the distribution of temperature in this example subset at each hour. Under clear and calm conditions, temperatures are tightly clustered around the mean with the most variability occurring in the first hour after sunset, which is generally the case for other stations and seasons.

To diminish the influence of the occasional outlier and the slightly higher variability in the first hour after sunset, robust linear regressions are fitted to the data in this example and illustrate the clear difference in cooling rates between the urban and the rural location. A simple linear regression shows similar results to the robust regression but gives a slightly greater difference between the cooling rates in high versus low urban fraction areas. Therefore, the robust fit actually provides a more conservative estimate of the difference, which is also the case for the subsequent results.

Cooling rates obtained from the slopes found from the robust regression are calculated for each station and each night over 2020–2022 whenever there is available data. When there is missing data, this leads to both temporal and spatial gaps in the sampling and can be treated in different ways. A strict approach would be to only use times and sensors where all data is available concurrently. Taking this approach substantially decreases the sample size, especially since many monitors have been installed recently. Another approach is to simply use all the available data, despite the different sampling in time and space. This approach is more inclusive, but it should be clearly stated that an underlying assumption is that there is no systematic bias as to which stations are active and when they are active. So, given the large amount of sensors in the region, there is expected to be random sampling over time and spatially, so a
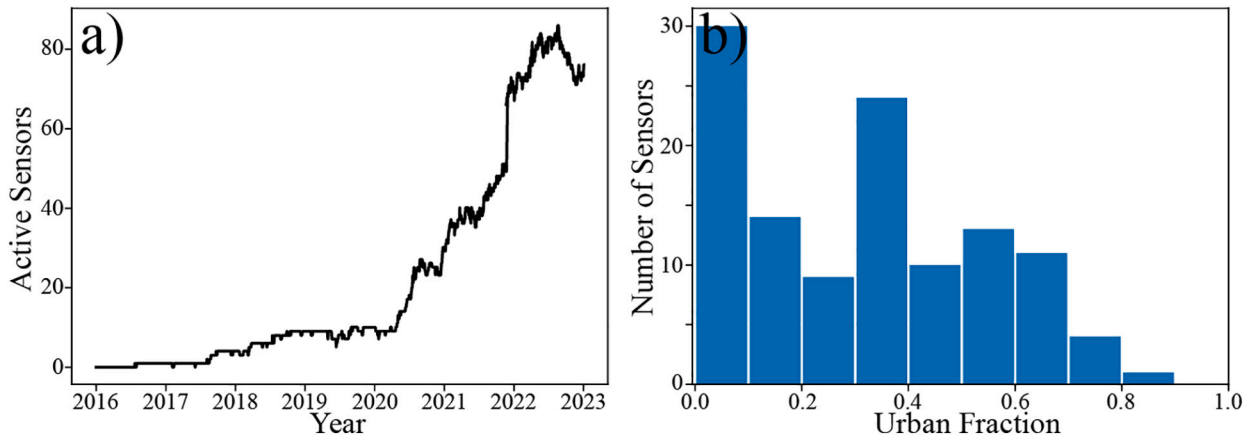
Fig. 1. (a) Number of concurrently active sensors and (b) histogram of urban fraction associated with all stations.
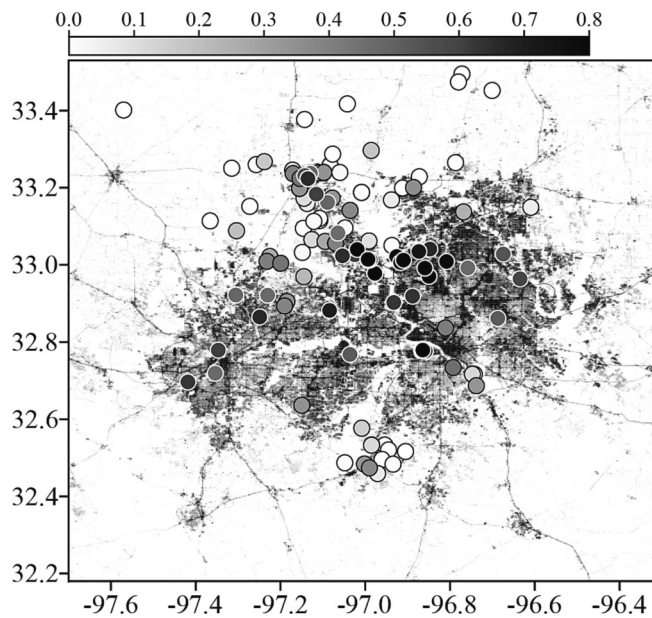

Fig. 2. The grayscale represents the urban fraction from the 30-m National Land Cover Database (Dewitz, 2021) and is defined by the percentage of urban impervious surface. The circles indicate the location of the monitors and the colour corresponds to the nearest urban fraction.

sampling bias should not be an issue. Given the nature of the data availability, the latter approach was used with the assumption that the data sampling is effectively random in space and time and there is no sampling bias.

4. Results

The spatial distribution of the mean cooling rates at each station during each season is illustrated in Fig. 5. At the regional scale, cooling rates are generally slower towards the more developed center of the city with rural stations towards the edges of the domain indicating distinctly faster cooling rates. For locations well away from any substantial urbanization, particularly in the rural areas located in the far northwest and northeast part of the domain, this is clearly and consistently the signal. Within the city, the heterogeneous nature of the built environment can create substantial differences in the local urban fraction over small scales and as a result the local cooling rates. It is at these small scales that having this type of fairly dense in situ measurements of air temperature is advantageous because it provides unprecedented information in a variety of locations within a complex environment. The mean cooling rates over the entire domain tend to be noticeably slower in the summer. Conclusions about general features in the other seasons are not easily interpreted from these spatial maps but can be obtained by taking several different approaches.

To further take advantage of this network and examine the impact of local conditions, each sensor's mean cooling rate as a function of its urban fraction in each season is depicted in Fig. 6. The figure indicates that the mean cooling rates slow as the urban fraction
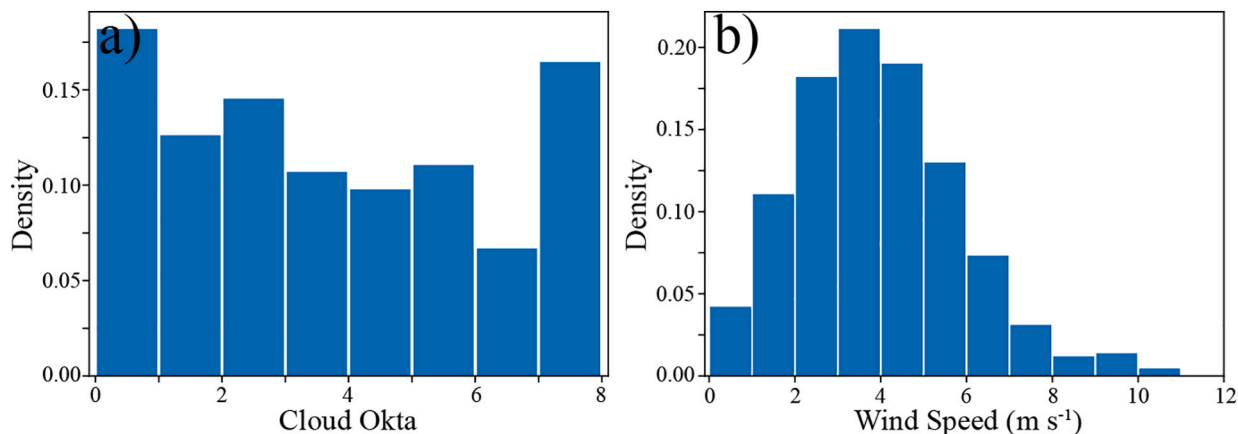
Fig. 3. The distributions of the 2020–2022 (a) cloud cover (okta) and (b) wind speed (m s^{-1}) averaged over the nocturnal window.
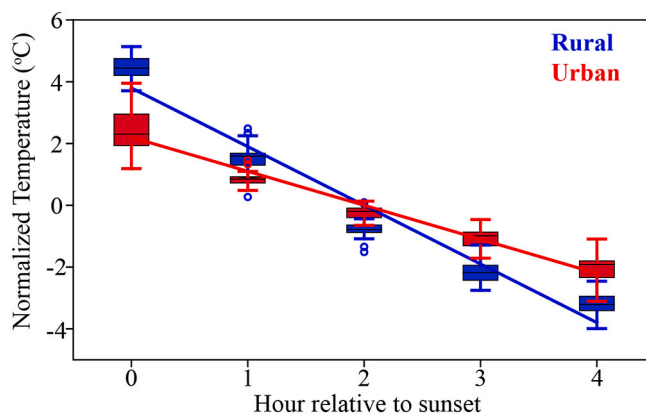

Fig. 4. The spring (MAM) 2020–2022 normalized air temperature (^{o}C) relative to sunset for a rural station (blue, urban fraction of 0.0) and an urban station (red, urban fraction of 0.6). Box plots show the interquartile range, whiskers extend 1.5 times the interquartile range, outliers are indicated as circles, and the black line is the median. Slopes are from the fitted robust linear regression. (For interpretation of the references to colour in this figure legend, the reader is referred to the web version of this article.)

increases and suggests that this is a linear relationship. A robust regression is applied and reveals that the cooling rate as a function of urban fraction is about 0.5–0.7 ^{o}C hr^{-1} urbfrac^{-1}. The steepest slopes of 0.7 ^{o}C hr^{-1} urbfrac^{-1} are present during the spring and fall, which means that the local built environment tends to have the greatest impact during these transitional seasons. The variability is greatest in the winter with a correlation coefficient dropping down to 0.2, while the other seasons are about 0.4. Despite more variability present in the winter, linear regressions during all seasons are significant at the 95% confidence level.

To highlight changes to the cooling rate distributions between high and low urban fractions, sensors are categorically separated above and below an urban fraction of 0.4 (Fig. 7). The reason for selecting this particular threshold is that this approximately separates 'open' from 'compact' built environments in the Local Climate Zone (LCZ) classification scheme (Stewart and Oke, 2012). Each category contains all available nightly cooling rates from each station.

The differences in the means of the distributions are all consistent with slower cooling rates where the urban fraction is greater, and all of the differences in the means are significant at the 95% level for all seasons. Each distribution is skewed such that there is a longer tail towards more rapid cooling rates. In the winter, the distributions of cooling rates are broader and more uniform, which is consistent with the highest variability in the station means (Fig. 6a), but there is still a significant difference in the mean of 0.33 ^{o}C hr^{-1} between the low and high urban fraction categories. Conversely, given that the lowest variability occurs in summer, the distributions of cooling rates are narrow with a difference of 0.24 ^{o}C hr^{-1}. The transitional seasons have similar distributions with a mean difference of 0.39 and 0.33 ^{o}C hr^{-1} in the spring and fall, respectively.

Mean differences of the distributions are further broken down by examining these at a monthly time scale for each individual year and over the entire 2020–2022 time period (Fig. 8). All months show that stations with a high urban fraction cool at a slower rate than low-urban fraction stations, even in 2020 when the sample size is low. The difference reaches a clear minimum in June with greater differences during the spring and fall. It is noted that this behavior is for a particular climate zone, but is consistent with seasonal surface heat island intensities (Manoli et al., 2020).
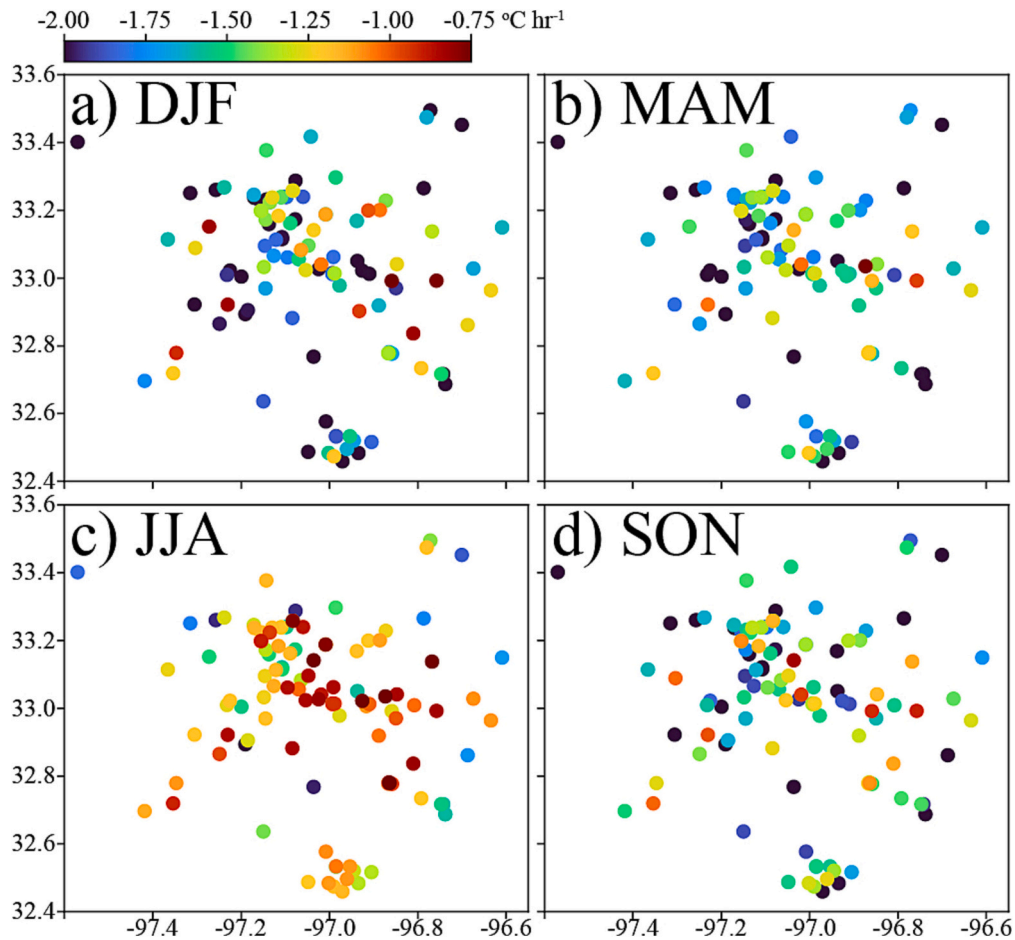
Fig. 5. Spatial distribution of cooling rates (°C hr⁻¹) for (a) DJF, (b) MAM, (c) JJA, and (d) SON.

5. Discussion

People living in urban areas are particularly susceptible to an accumulation of adverse health and economic impacts, but these impacts are not evenly distributed throughout a city. The impact of the UHI is often examined at the city level using surface temperature from satellite observations, and while this gives good information, there is an assortment of limitations related to this type of approach as summarized in Stewart et al. (2021). The great need for more data has recently motivated substantial investment in UHI mapping campaigns in major US cities that mobilize citizen scientists to drive through their neighborhoods and collect data (Zabow et al., 2023). While these measurements provide excellent spatial data, these are obtained over just one day. To address some of the limitations, specifically those related to the heterogeneous temperature response within a city over many days and the difference between satellite surface temperature and air temperature, a relatively dense network of in situ air temperature measurements is required.

There is a growing number of low-cost sensors installed in cities from different networks (e.g., Gubler et al., 2021; Barkjohn et al., 2021). These low-cost sensor networks are expanding globally and are especially important in regions such as Latin America, Africa, and south Asia that are underrepresented in UHI studies (Stewart, 2011). The PurpleAir network has the primary impetus of monitoring air pollution but also concurrently provides a much-needed increase in the number of temperature measurements at the neighborhood level. Given the increase of the background air temperature associated with climate change coupled with enhanced local warming from the UHI effect, being able to measure the temperature distribution through the city is valuable, especially overnight temperatures that can lead to increased morbidity, mortality, and higher energy costs for air conditioning. These networks are already being used to support communities concerned about air pollution, and better information on the local UHI impact will be able to support advocacy in the broader environmental justice movement (Proma et al., 2021; Boston et al., 2023).

To constrain the study, the Dallas-Fort Worth region is selected because it provides an excellent area to investigate local impacts of the built environment on the overnight cooling rates of air temperature. The influence of significant weather events is removed by selecting only calm and clear nights to isolate the local effects on cooling rates. Despite the varying form and function of the built environment, the urban fraction (defined as the percentage of urban impervious surface in the National Land Cover Database) provides
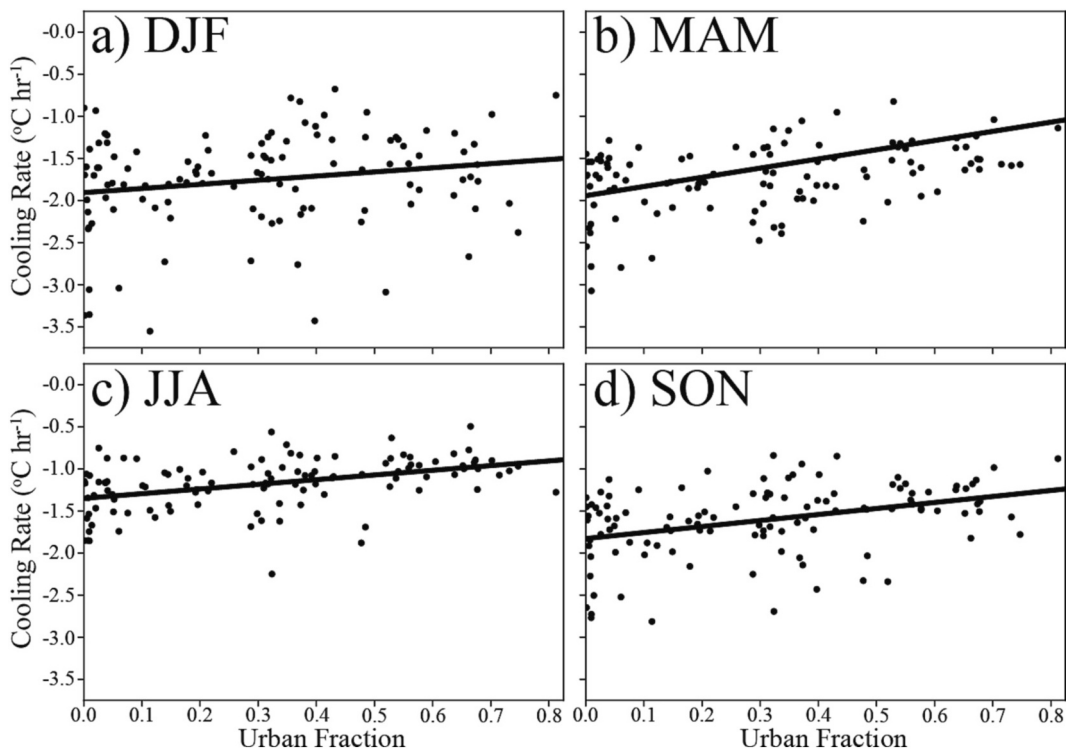
Fig. 6. Cooling rate (°C hr⁻¹) as a function of urban fraction for (a) DJF, (b) MAM, (c) JJA, and (d) SON.
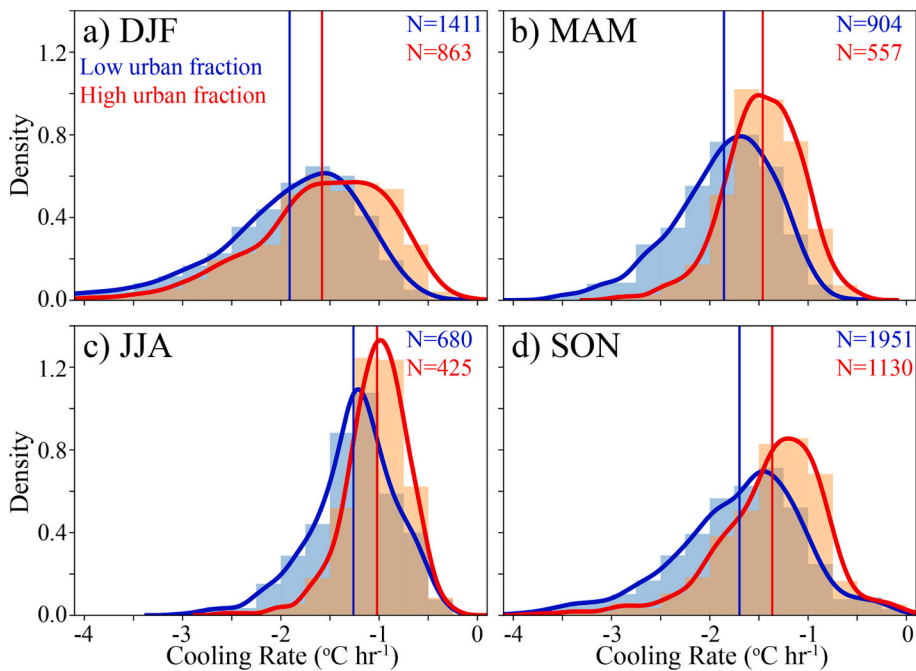

Fig. 7. Probability density function of cooling rates (°C hr⁻¹) above (red) and below (blue) an urban fraction of 0.4 during (a) DJF, (b) MAM, (c) JJA, and (d) SON. Vertical lines indicate the mean of each distribution, and the sample size of each distribution is indicated in the upper right of each panel. (For interpretation of the references to colour in this figure legend, the reader is referred to the web version of this article.)
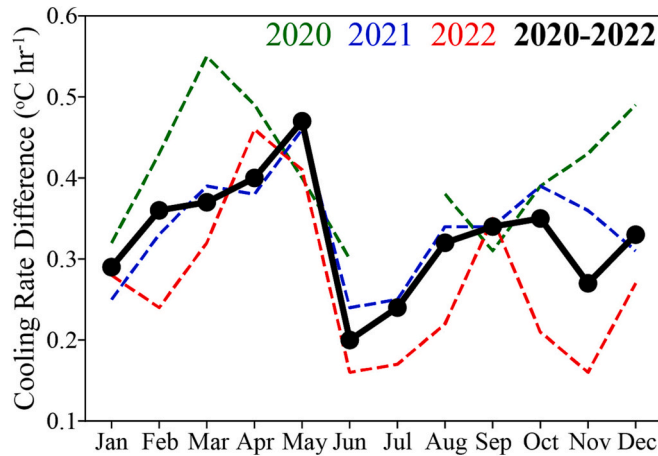
Fig. 8. Differences of cooling rates (^{o}C hr^{-1}) corresponding to urban fractions above 0.4 minus urban fractions below 0.4 for each month in 2020 (green), 2021 (blue), 2022 (red), and grouped by month for all years (black). (For interpretation of the references to colour in this figure legend, the reader is referred to the web version of this article.)

a simple but effective way to assess the degree of impact that urbanization has on the air temperature.

Cooling rates slow towards the generally more developed urban centers of Dallas-Fort Worth, but the small-scale variability even from locations relatively close to one another reveals the spatial variability present in the city that is captured by this measurement network (Fig. 5). When the cooling rates are related to their local urban fraction, a significant linear relationship is revealed in all seasons with values of 0.5–0.7 ^{o}C hr^{-1} urbfrac^{-1}. Winter months exhibit the highest variability of the station's cooling rates as a function of urban fraction. For studies that are concerned about warm season issues like heat-related illnesses and energy usage related to air conditioning, the winter variability is not particularly concerning. However, slow cooling rates in the winter are actually advantageous since warmer temperatures mean less energy is used for heating.

The variability in any given urban fraction category can be attributed to several factors. Urban fraction is a single way to represent the surrounding built environment and does not contain specific information about its form or function, which may have different impacts on the cooling rates. Alternative classifications such as using LCZs provide slightly better representations of land use, but even in the LCZ categorical approach, there are still ranges of building form and function within each category. Also, although these findings are for nights that the wind is relatively calm, modest temperature advection can still occur and the footprint outside the nearest neighbor classification may exert some influence. This could explain why there is a tail towards rapid cooling rates. For example, if the area just upwind is a low urban fraction, then the cooling rates at the higher urban fraction just downwind could also be higher.

Other weather and climate factors also contribute to the variability. For instance, soil moisture can change the energy partitioning drastically and greatly impact the nocturnal cooling rates. This is not captured by discriminating by just clear or calm conditions, since the area could be in drought conditions or wet conditions. Furthermore, irrigation in urban areas can also modify the surface characteristics outside of natural causes occurring ubiquitously over the broader region.

Even with many things potentially contributing to the variability, the overall relationship between cooling rates and urban fraction is clear and has been shown to be significant. The spatial coverage is currently better than standard observing networks, but the length of the time series is still relatively short. This means that accounting more broadly for weather and climate factors is still challenging at the moment since the sample size for particular weather and climate conditions is small. However, as the number of measurements continues to increase even over just the next few years, these questions will be able to be addressed. A longer time record will include more variability in weather conditions and will help address more refined questions such as how drought or ample rain impacts the cooling rates in different parts of the city and in the adjacent rural areas.

The large number of new low-cost sensors, which are not just PurpleAir in the Dallas-Fort Worth region, include many other systems worldwide that will provide a promising avenue for continued refinement of linking the built environment to neighborhood-level characteristics that have previously been examined with remote sensing, which has its own drawbacks. Questions of local climate in the cooling rate response can be quantified with this dataset to complement more global studies such as Manoli et al. (2020) that investigate the UHI hysteresis. Spatial and time scales of these studies can generally be categorized into (1) more climate-like studies that examine long-term averages of the distribution of a city's UHI or compare the variation of city-scale UHI intensity of many different cities and account for climatic zone variability, and into (2) neighborhood-scale examination at shorter times scales such as the UHI response during a heatwave. There are merits to both approaches and advances can be made by approaching the issue from both perspectives, with the intent of bridging the gaps in scale as advocated by Or (2020). In fact, Manoli et al. (2020) also advocate for a shift from urban climate to urban weather studies that better relate how synoptic conditions interact with urban areas.

6. Conclusion

Air temperature is available in low-cost air pollution monitor networks, but these are underused observations that can complement other low-cost weather networks (e.g, Netatmo and WeatherFlow) and remotely sensed surface temperatures to investigate local cooling rates as a function of urban fraction. For community stakeholders, this means temperature observations can be readily incorporated into their existing work that is focused on air pollution, especially in under-served communities. Since cooling rates are interpreted through urban fractions, these results can be readily used to highlight that a lack of green space (a high urban fraction) significantly alters local temperatures. This is not a new concept (Harlan et al., 2007), but local data is still necessary to back up any community advocacy if it is to lead to real change (Boston et al., 2023). There are also educational benefits to the community through the use of their own data, which is one motivation behind large mulit-city UHI mapping projects (Zabow et al., 2023). This study demonstrates a significant correlation between the cooling rate and urban fraction, which varies in intensity with the meteorological season.

Before committing to more universal studies using these low-cost sensor networks, additional work on local variability at the city scale should be conducted to further leverage this network for applications related to the UHI. Having data readily available for community groups is one of many ways to support current initiatives to raise awareness and promote actionable mitigation strategies of the UHI. Continued investment in low-cost sensors in underserved areas will support these initiatives.

Declaration of competing interest

- The authors declare that they have no known competing financial interests or personal relationships that could have appeared to influence the work reported in this paper.
- The authors declare the following financial interests/personal relationships which may be considered as potential competing interests:

Data availability

Publicly available from https://api.purpleair.com.

Acknowledgement

References

Akbari, H., Pomerantz, M., Taha, H., 2001. Cool surfaces and shade trees to reduce energy use and improve air quality in urban areas. Sol. Energy 70, 295–310.

Arnfield, A.J., 2003. Two decades of urban climate research: a review of turbulence, exchanges of energy and water, and the urban heat island. Int. J. Climatol. 23, 1–26.

Azevedo, J.A., Chapman, L., Muller, C.L., 2016. Quantifying the daytime and night-time urban heat island in Birmingham, Uk: a comparison of satellite derived land surface temperature and high resolution air temperature observations. Remote Sens. 8, 153.

Barkjohn, K.K., Gantt, B., Clements, A.L., 2021. Development and application of a United States-wide correction for PM2.5 data collected with the PurpleAir sensor. Atmos. Meas. Tech. 14, 4617–4637. https://doi.org/10.5194/amt-14-4617-2021.

Basara, J.B., Hall, P.K., Schroeder, A.J., Illston, B.G., Nemunaitis, K.L., 2008. Diurnal cycle of the Oklahoma City urban heat island. J. Geophys. Res. Atmos. 113, 1–16. https://doi.org/10.1029/2008JD010311.

Boston, P.Q., Strouble, B., Balogun, A., Lugo-Martinez, B., McClain, M., Mitchell, M.M., Wasserman, K., Rahn, D., Greenberg, M., Garibay, C., 2023. Community voices on the experiences of community-based participatory research in the environmental justice movement. Sociol. Sci. 12, 358.

Chakraborty, T., Hsu, A., Manya, D., Sheriff, G., 2019. Disproportionately higher exposure to urban heat in lower-income neighborhoods: a multi-city perspective. Environ. Res. Lett. 14, 105003. URL: https://iopscience.iop.org/article/10.1088/1748-9326/ab3b99, doi: https://doi.org/10.1088/1748-9326/ab3b99.

Chapman, L., Bell, C., Bell, S., 2017. Can the crowdsourcing data paradigm take atmospheric science to a new level? A case study of the urban heat island of London quantified using Netatmo weather stations. Int. J. Climatol. 37, 3597–3605. https://rmets.onlinelibrary.wiley.com/doi/10.1002/joc.4940. https://doi.org/10.1002/joc.4940.

Dewitz, J., . National Land Cover Database (Nlcd) 2019 Products. URL: https://www.sciencebase.gov/catalog/item/5f21cef582cef313ed940043. https://doi.org/10.5066/P9KZCM54.

Gubler, M., Christen, A., Remund, J., Brönnimann, S., 2021. Evaluation and application of a low-cost measurement network to study intra-urban temperature differences during summer 2018 in Bern. Switzerland. Urban Climate 37. https://doi.org/10.1016/j.uclim.2021.100817.

Hafner, J., Kidder, S.Q., 1999. Urban heat island modeling in conjunction with satellite-derived surface/soil parameters. J. Appl. Meteorol. 38, 448–465.

Harlan, S.L., Brazel, A.J., Darrel Jenerette, G., Jones, N.S., Larsen, L., Prashad, L., Stefanov, W.L., 2007. In the shade of affluence: the inequitable distribution of the urban heat island. Res. Soc. Probl. and Pub. Poli. 15, 173–202. https://doi.org/10.1016/S0196-1152(07)15005-5.

He, W., Li, X., Zhou, Y., Shi, Z., Yu, G., Hu, T., Wang, Y., Huang, J., Bai, T., Sun, Z., Liu, X., Gong, P., 2023. Global urban fractional changes at a 1 km resolution throughout 2100 under eight scenarios of shared socioeconomic pathways (SSPs) and representative concentration pathways (RCPs). Earth Sys. Sci, Data 15, 3623–3639. URL: https://essd.copernicus.org/articles/15/3623/2023/ https://doi.org/10.5194/essd-15-3623-2023.

Heaviside, C., Vardoulakis, S., Cai, X.M., 2016. Attribution of mortality to the urban heat island during heatwaves in the west midlands. UK. Environ, Health 15, S27.

Hu, L., Brunsell, N.A., 2013. The impact of temporal aggregation of land surface temperature data for surface urban heat island (suhi) monitoring. Remote Sens. Environ. 134, 162–174.

Hu, L., Brunsell, N.A., 2015. A new perspective to assess the urban heat island through remotely sensed atmospheric profiles. Remote Sens. Environ. 158, 393–406.

Huber, P., Ronchetti, E., 2011. Robust Statistics. Wiley Series in Probability and Statistics,. Wiley.

Imhoff, M.L., Zhang, P., Wolfe, R.E., Bounoua, L., 2010. Remote sensing of the urban heat island effect across biomes in the continental Usa. Remote Sens. Environ. 114, 504–513.

Laaidi, K., Zeghnoun, A., Dousset, B., Bretin, P., Vandentorren, S., Giraudet, E., Beaudeau, P., 2012. The impact of Heat Islands on mortality in Paris during the august 2003 heat wave. Environ. Health Perspect. 120, 254–259.

Malings, C., Tanzer, R., Hauryliuk, A., Saha, P.K., Robinson, A.L., Presto, A.A., Subramanian, R., 2020. Fine particle mass monitoring with low-cost sensors: corrections and long-term performance evaluation. Aerosol Sci. Technol. 54, 160–174. https://doi.org/10.1080/02786826.2019.1623863.

Manoli, G., Fatichi, S., Bou-Zeid, E., Katul, G.G., 2020. Seasonal hysteresis of surface urban heat islands. Proc. Natl. Acad. Sci. 117, 7082–7089.

Monaghan, A.J., Hu, L., Brunsell, N.A., Barlage, M., Wilhelmi, O.V., 2014. Evaluating the impact of urban morphology configurations on the accuracy of urban canopy model temperature simulations with modis. J. Geophys. Res. Atmos. 119, 6376–6392.

Morris, C., Simmonds, I., 2000. Associations between varying magnitudes of the urban heat island and the synoptic climatology in Melbourne, Australia. Int. J. Climatol. 20, 1931–1954.

Myrup, L., McGinn, C., Flocchini, R., 1993. An analysis of microclimatic variation in a suburban environment. Atmospheric Environment. Part B. Urban Atmosphere 27, 129–156.

Nielsen, K.F., Rahn, D.A., 2022. Morning transition of the boundary layer over Dallas–fort worth. J. Appl. Meteorol. Climatol. 61, 1433–1448.

Oke, T., 1982. The energetic basis of the urban heat island. Q. J. R. Meteorol. Soc. 108, 1–24. https://doi.org/10.1002/qj.49710845502.

Oke, T., 1988. The urban energy balance. Prog. Phys. Geogr. 12, 471–508.

Oke, T., 1995. The Heat Island of the Urban Boundary Layer: Characteristics, Causes and Effects, In: Wind Climate In Cities. Springer, pp. 81–107.

Or, D., 2020. The tyranny of small scales—on representing soil processes in global land surface models. Water Resour. Res. 56.

Peng, S., Piao, S., Ciais, P., Friedlingstein, P., Ottle, C., Breon, F.M., Nan, H., Zhou, L., Myneni, R.B., 2011. Surface urban heat island across 419 global big cities. Environ. Sci. Technol. 46, 696–703.

Proma, R.A., Sumpter, M., Lugo, H., Friedman, E., Huq, K.T., Rosen, P., 2021. Cleanairnowkc: building community power by improving data accessibility, in: 2021 IEEE workshop on visualization for social good (VIS4Good). IEEE 1–5.

Salamanca, F., Georgescu, M., Mahalov, A., Moustaoui, M., Wang, M., 2014. Anthropogenic heating of the urban environment due to air conditioning. J. Geophys. Res. Atmos. 119, 5949–5965.

Shahmohamadi, P., Che-Ani, A., Maulud, K., Tawil, N., Abdullah, N., 2011. The impact of anthropogenic heat on formation of urban heat island and energy consumption balance. Urban Studies Res. 2011.

Stavroulas, I., Grivas, G., Michalopoulos, P., Liakakou, E., Bougiatioti, A., Kalkavouras, P., Fameli, K., Hatzianastassiou, N., Mihalopoulos, N., Gerasopoulos, E., 2020. Field evaluation of low-cost PM sensors (purple air PA-II) under variable urban air quality conditions, in Greece. Atmosphere 11, 926. URL: https://www.mdpi.com/2073-4433/11/9/926 https://doi.org/10.3390/atmos11090926.

Stewart, I.D., 2011. A systematic review and scientific critique of methodology in modern urban heat island literature. Int. J. Climatol. 31, 200–217. https://rmets.onlinelibrary.wiley.com/doi/10.1002/joc.2141 https://doi.org/10.1002/joc.2141.

Stewart, I.D., Oke, T.R., 2012. Local climate zones for urban temperature studies. Bull. Am. Meteorol. Soc. 93, 1879–1900.

Stewart, I., Krayenhoff, E., Voogt, J., Lachapelle, J., Allen, M., Broadbent, A., 2021. Time evolution of the surface urban heat island. Earth's. Future 9 e2021EF002178.

Tran, H., Uchihama, D., Ochi, S., Yasuoka, Y., 2006. Assessment with satellite data of the urban heat island effects in asian mega cities. Int. J. Appl. Earth Obs. Geoinf. 8, 34–48.

Unwin, D.J., 1980. The synoptic climatology or birmingham's urban heat island, 1965-1974. Weather 35, 43–50.

Weng, Q., Rajasekar, U., Hu, X., 2011. Modeling urban heat islands and their relationship with impervious surface and vegetation abundance by using aster images. IEEE Trans. Geosci. Remote Sens. 49, 4080–4089.

Wong, M.M.F., Fung, J.C.H., Yeung, P.P.S., 2019. High-resolution calculation of the urban vegetation fraction in the Pearl River Delta from the Sentinel-2 NDVI for urban climate model parameterization. Geosci. Lett. 6, 2. https://doi.org/10.1186/s40562-019-0132-4.

Zabow, M., Jones, H., Trtanj, J., McMahon, K.G., Schramm, P., 2023. The national integrated heat health information system: a federal approach to addressing extreme heat and health, in: 103rd AMS annual meeting. AMS 5, 6.

Zhang, Y., Gao, Z., Li, D., Li, Y., Zhang, N., Zhao, X., Chen, J., 2014. On the computation of planetary boundary-layer height using the bulk Richardson number method. Geosci. Model Dev. 7, 2599–2611. https://doi.org/10.5194/gmd-7-2599-2014.